

CONVERTED WAVE REVERSE TIME MIGRATION WITH GAUSSIAN BEAMS IN VTI MEDIA

JIAN-EN XIAO¹, ZHEN-CHUN LI^{1,2}, KAI ZHANG^{1,2} and QIANG LIU¹

¹ School of Geosciences, China University of Petroleum (East China), Qingdao 266580, P.R. China. 359974117@qq.com

² Evaluation and Detection Technology Laboratory of marine mineral resources, Qingdao National Laboratory for Marine Science and Technology, Qingdao 266071, P.R. China.

(Received April 25, 2018; revised version accepted April 12, 2019)

ABSTRACT

Xiao, J.E., Li, Z.C., Zhang, K. and Liu, Q., 2019. Converted wave reverse time migration with Gaussian beams in VTI media. *Journal of Seismic Exploration*, 28: 205-220.

With the development of seismic data acquisition technology, more and more multi-component seismic data are being acquired. Owing to the slow propagation velocity and wide propagation angle, the converted PS-wave contains more accurate subsurface information, which make it play an important role in multi-component seismic exploration. Compared with the P-wave, the converted PS-wave is more sensitive to the anisotropy, which cannot be neglected during the seismic migration. Reverse time migration with Gaussian beams combines the high calculation efficiency of Gaussian beam migration and the high imaging accuracy of reverse time migration, which can be used for the converted PS-wave imaging. In this paper, we derive the converted PS-wave ray tracing equations based on phase velocity and present the imaging condition of converted PS-wave, then we propose a converted wave reverse time migration with Gaussian beams method for VTI media. The numerical tests on anisotropic models demonstrate the effectiveness and applicability of the proposed method.

KEY WORDS: converted wave, reverse time migration, Gaussian beams, VTI media.

INTRODUCTION

In recent years, the exploration target has been gradually turned to multi-component seismic exploration with the development of seismic data acquisition technology. The multi-component exploration technology also has been developed rapidly, especially the converted PS-wave technology. The anisotropy widely exists in subsurface media. The use of traditional isotropic migration methods to process the seismic data of anisotropic areas will lead to the problems such as the inability to locate reflected waves accurately, the incomplete convergence of diffraction waves and the lack of energy focus, which will adversely affect the migration velocity analysis and reservoir prediction. The converted PS-wave is typically more affected by the anisotropy compared with the P-wave. It is necessary to develop a converted PS-wave imaging method applicable to anisotropic media.

The current converted wave imaging methods can be divided into three categories: (a) the common converted point (referred to as CCP) horizontal stacking method (Tessmer G et al., 1990; Ma, 1995); (b) converted PS-wave dip-moveout correction (DMO) (Rooijen, 1991; Alfaraj and Lerner, 1992); (c) converted PS-wave pre-stack migration technology. With the increasing complexity of exploration targets, the CCP and DMO methods could no longer meet the exploration requirements of complex structural exploration areas. The pre-stack migration consists of pre-stack time migration (Wang et al., 2002; Dai and Li, 2006; Li et al., 2007) and pre-stack depth migration. As a key imaging technology for the areas with strong lateral velocity change and complex structures, the pre-stack depth migration methods have gradually become the research hotspots. The pre-stack depth migration methods can be further divided into the ray methods and the wave-equation methods.

The ray methods are characterized by the high efficiency and flexibility. As an improved ray method, Gaussian beam migration not only inherits the flexibility and efficiency of Kirchhoff migration (Hill, 1990, 2001; Nowack et al., 2003; Gray, 2005; Gray and Bleistein, 2009), but also overcomes the inherent defects of Kirchhoff migration, such as caustics, shadows, and multiple arrivals (Yue, 2011). Alkihalifah (1995) extended the poststack Gaussian beam migration to anisotropic media by deriving the anisotropic kinematic and dynamic ray tracing equations. Zhu et al. (2005, 2007) implemented the anisotropic prestack Gaussian beam migration by redefining the anisotropic kinematic and dynamic ray tracing equations based on phase velocity. Han et al. (2014) proposed a Gaussian beam prestack depth migration of converted PS-wave in TI media by introducing the anisotropic ray tracing systems based on elastic parameters.

The wave-equation methods consist of the methods based on one-way wave equation (Yu et al., 2007; Sun et al., 2010) and the methods based on two-way wave equation (referred to as reverse time migration) (Baysal et al., 1983; Guitton et al., 2006). The methods based on one-way wave equation have a higher imaging accuracy than that of the ray methods, but they cannot deal with the imaging problems of steeply inclined structures. Reverse time

migration implements the backward continuation of seismic wavefields in the time direction, then the imaging results are obtained by the cross-correlation of forward and backward continuation wavefields. It overcomes the limit of steep dips, but it has a higher requirement for velocity field and computer hardware.

Based on Kirchhoff integral, Popov et al. (2010) proposed a reverse time migration algorithm that adopted the weighted superposition of Gaussian beams to construct the Green function. Huang et al. (2014) used the Green function represented by Gaussian beams to implement the forward and backward continuation of seismic wavefields, then realized the reverse time migration with Gaussian beams. Zhang et al. (2015) presented an angle-domain reverse time migration with Gaussian beams in VTI media by introducing the anisotropic ray tracing equations based on elastic parameters. Bi et al. (2015) realized the elastic reverse time migration with Gaussian beams that combined the high imaging accuracy of elastic wave reverse time migration and the high computational speed of elastic Gaussian beam migration.

In this paper, we present a converted wave reverse time migration with Gaussian beams method for VTI media. We develop an anisotropic converted PS-wave ray tracing algorithm: the P-wave ray tracing equation and SV-wave ray tracing equation are used at source and receiver, respectively. Then we construct the Green function by the elastic wave Gaussian beams, finally the imaging results are obtained by the cross-correlation of forward and backward continuation wavefields. The numerical tests on anisotropic models demonstrate the effectiveness and applicability of the proposed method. The algorithm proposed by this paper is more concise and has a higher computational efficiency than the anisotropic algorithm based on elastic parameters.

THEORY

Anisotropic converted wave ray tracing based on phase velocity

The path and traveltimes of the central ray are obtained by the kinematic ray tracing, while the dynamic parameters P and Q are calculated by dynamic ray tracing.

Kinematic ray tracing

Červený (1972) presented the anisotropic kinematic ray tracing equation based on elastic parameters, but the computational efficiency was relatively low and the eigenvalues needed to be calculated at each step of ray tracing. To solve these problems, Zhu et al. (2005, 2007) redefined the anisotropic kinematic ray tracing equation based on phase velocity. Here we generalize it to the converted PS-wave ray tracing in anisotropic media, which can be expressed as follows:

$$\begin{cases} \frac{dx_i}{d\tau} = V_{Pi}, \frac{dp_{Pi}}{d\tau} = -\frac{1}{v_P} \frac{\partial v_P}{\partial x_i} \\ \frac{dx_i}{d\tau} = V_{Si}, \frac{dp_{Pi}}{d\tau} = -\frac{1}{v_S} \frac{\partial v_S}{\partial x_i} \end{cases}, \quad (1)$$

where V_{Pi} and V_{Si} are the group velocities of P-wave and SV-wave, respectively. v_P and v_S are the phase velocities of P-wave and SV-wave, respectively, they take the form:

$$\begin{cases} v_P = v_{P0}(1 + \delta \sin^2 \theta \cos^2 \theta + \varepsilon \sin^4 \theta) \\ v_S = v_{S0}(1 + \sigma \sin^2 \theta \cos^2 \theta) \end{cases}, \quad (2)$$

where ε and δ are the Thomsen (1986) anisotropic parameters, v_{P0} and v_{S0} are the vertical velocities of P-wave and SV-wave, θ is the angle of phase velocity, σ takes the form:

$$\sigma = (\varepsilon - \delta) \frac{v_{P0}^2}{v_{S0}^2}. \quad (3)$$

Dynamic ray tracing

The ray center coordinate system was no longer orthogonal in anisotropic media, and a weight variable along the ray path needed to be introduced to eliminate the impact of this non-orthogonality. Hanyga (1986) gave the anisotropic dynamic ray tracing equation based on the elastic parameters. But they were too complicated to calculate and the weak anisotropic parameters of the subsurface media should be specified. Zhu et al. (2005, 2007) derived the anisotropic dynamic ray tracing equation based on phase velocity. For anisotropic converted PS-wave ray tracing, it takes the form:

$$\begin{cases} \frac{dP_{PM}}{d\tau} = -A_{MN}Q_{PN} - B_{MN}P_{PN} \\ \frac{dQ_{PN}}{d\tau} = C_{MN}Q_{PN} + D_{MN}P_{PN} \end{cases}, \begin{cases} \frac{dP_{SM}}{d\tau} = -A'_{MN}Q_{SN} - B'_{MN}P_{SN} \\ \frac{dQ_{SN}}{d\tau} = C'_{MN}Q_{SN} + D'_{MN}P_{SN} \end{cases}, \quad (4)$$

where P and Q are the dynamic ray tracing parameters, $A_{MN}, B_{MN}, C_{MN}, D_{MN}$ are the correlation coefficients, which can be expressed as:

$$\left\{ \begin{array}{l} A_{MN} = \frac{1}{v_P} \frac{\partial^2 v_P}{\partial y_M \partial y_N}, B_{MN} = \frac{\partial^2 \ln v_P}{\partial y_M \partial y_N} \\ C_{MN} = \frac{\partial^2 \ln v_P}{\partial y_N \partial q_M}, D_{MN} = \frac{\partial V_{PN}}{\partial q_M} \end{array} \right\}, \left\{ \begin{array}{l} A'_{MN} = \frac{1}{v} \frac{\partial^2 v_S}{\partial y_M \partial y_N}, B'_{MN} = \frac{\partial^2 \ln v_S}{\partial y_M \partial y_N} \\ C'_{MN} = \frac{\partial^2 \ln v_S}{\partial y_N \partial q_M}, D'_{MN} = \frac{\partial V_{SN}}{\partial q_M} \end{array} \right\}, \quad (5)$$

where y_M and y_N are the coordinates of the ray center coordinate system,

$$q_M = \frac{\partial \tau}{\partial y_M}.$$

The continuation of seismic wavefields

Fig. 1 displays the 2D ray center coordinate system. \mathbf{n} and \mathbf{t} are the two base vectors of the coordinate system. \mathbf{n} is the unit vector that is perpendicular to the ray and points to the same side of the ray. \mathbf{t} is the unit vector tangent to the ray.

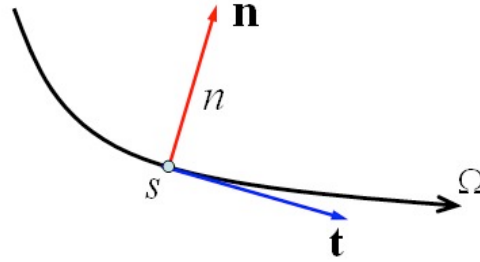


Fig. 1. 2D ray center coordinate system.

According to the solution of 2D parabolic wave equation (Babic, 1980; Červený, 1982), the Gaussian beam displacement formulas of P-wave and SV-wave take the form:

$$\left\{ \begin{array}{l} \mathbf{u}_p(s, n, \omega, t) = \frac{\Psi_p}{\sqrt{v_p(s)\rho(s)q(s)}} \left[\mathbf{t} + \frac{np(s)v_p(s)}{q(s)} \mathbf{n} \right] \exp \left\{ -i\omega \left[t - \int_0^s \frac{ds}{v_p(s)} - \frac{1}{2} \frac{p(s)}{q(s)} n^2 \right] \right\} \\ \mathbf{u}_{sv}(s, n, \omega, t) = \frac{\Psi_{sv}}{\sqrt{v_{sv}(s)\rho(s)q(s)}} \left[\mathbf{n} - \frac{np(s)v_{sv}(s)}{q(s)} \mathbf{t} \right] \times \exp \left\{ -i\omega \left[t - \int_0^s \frac{ds}{v_{sv}(s)} - \frac{1}{2} \frac{p(s)}{q(s)} n^2 \right] \right\} \end{array} \right\}, \quad (6)$$

where $\mathbf{u}_p(s, n, \omega, t)$ and $\mathbf{u}_{sv}(s, n, \omega, t)$ are the displacements of P-wave and SV-wave, respectively, Ψ_p and Ψ_{sv} are the weighting coefficients. $p(s)$ and $q(s)$ are the dynamic ray tracing parameters, $v_p(s)$ and $v_{sv}(s)$ are the velocities of P-wave and SV-wave, respectively, $\rho(s)$ is the density.

The displacement vector $U_m(\mathbf{x}_s; \mathbf{x}; \omega)$ aroused by the source point \mathbf{x}_s can be obtained by the superposition of elastic Gaussian beams that exits from \mathbf{x}_s with different emergence angles, which can be written as:

$$U_m^n(\mathbf{x}_s; \mathbf{x}; \omega) \approx \Psi^n \int \frac{dp_x(\mathbf{x}_s)}{p_z(\mathbf{x}_s)} u_m^n(\mathbf{x}_s; \mathbf{x}; \omega), \quad (7)$$

where $p_x(\mathbf{x}_s)$ and $p_z(\mathbf{x}_s)$ are the horizontal and vertical components of the initial ray parameter, $u_m(\mathbf{x}_s; \mathbf{x}; \omega)$ is the Gaussian beam wavefield of P-wave or SV-wave, n represents P-wave or SV-wave, Ψ^n is the weighting coefficient, it takes the form:

$$\Psi^n = \frac{i}{4\pi (v^n(\mathbf{x}_s))^2} \sqrt{\frac{\omega_r w_0^2}{\rho(\mathbf{x}_s)}}, \quad (8)$$

where $v^n(\mathbf{x}_s)$ is the velocity of P-wave or SV-wave, w_0 is the initial width of the Gaussian beam, ω_r is the reference frequency.

Pao (1976) derived the elastic wave Kirchhoff-Helmholtz integral equation of isotropic media. After neglecting the physical term, we can obtain the backward continuation elastic wave displacement vector wavefield at time t_0 :

$$u_m(\mathbf{x}; \mathbf{x}_r; t_0) = \int_{t_0}^T dt \int_S ds \left[t_i(\mathbf{x}_r, t) G_{lm}(\mathbf{x}_r, t; \mathbf{x}, t_0) - u_i(\mathbf{x}_r, t) \sum_{lm}(\mathbf{x}_r, t; \mathbf{x}, t_0) \right], \quad (9)$$

where $u_i(\mathbf{x}_r, t)$ is the elastic wave seismic records received on the surface, S is a closed surface that surrounds a region. $t_i(\mathbf{x}_r, t)$ is the stress at \mathbf{x}_r , $G_{lm}(\mathbf{x}_r, t; \mathbf{x}, t_0)$ and $\sum_{lm}(\mathbf{x}_r, t; \mathbf{x}, t_0)$ are the Green displacement tensor and stress tensor, respectively, they take the form:

$$\left\{ \begin{array}{l} t_i = n_j C_{ijkl} \frac{\partial u_l}{\partial x_k} \\ C_{ijkl} = \delta_{ij} \delta_{kl} \lambda(\mathbf{x}) + (\delta_{ik} \delta_{jl} + \delta_{il} \delta_{jk}) \mu(\mathbf{x}) \\ G_{lm}(\mathbf{x}; \mathbf{x}_r; \omega) = \sum_n g_{lm}^n(\mathbf{x}; \mathbf{x}_r; \omega) \\ \sum_{lm} = C_{ijkl} n_j \frac{\partial G_{lm}}{\partial x_k} \end{array} \right. , \quad (10)$$

where n_j is the unit vector that is perpendicular to the integral surface and points to the normal direction, C_{ijkl} is the stress tensor. δ is the Kronecker Delta function, λ and μ are the lame elastic parameters, $g_{lm}^n(\mathbf{x}; \mathbf{x}_r; \omega)$ is the Green function of P-wave or SV-wave.

Assuming that S is the free surface (the free stress boundary conditions take the form: $t(x; \omega) = 0, x \in S(z = 0); n_j = (0, -1)$), eq. (9) can be simplified as:

$$\begin{aligned} u_m(\mathbf{x}; \mathbf{x}_r; t_0) = & \int_{t_0}^T dt \int_S dx_r \left\{ u_x(\mathbf{x}; \omega) \mu(\mathbf{x}_r) \left[\frac{\partial g_{xm}^*(\mathbf{x}_r, t; \mathbf{x}, t_0)}{\partial x_2} + \frac{\partial g_{zm}^*(\mathbf{x}_r, t; \mathbf{x}, t_0)}{\partial x_1} \right] \right. \\ & \left. + u_z(\mathbf{x}_r; \omega) \left[[\lambda(\mathbf{x}_r) + 2\mu(\mathbf{x}_r)] \frac{\partial g_{zm}^*(\mathbf{x}_r, t; \mathbf{x}, t_0)}{\partial x_2} + \lambda(\mathbf{x}_r) \frac{\partial g_{xm}^*(\mathbf{x}_r, t; \mathbf{x}, t_0)}{\partial x_1} \right] \right\}, \end{aligned} \quad (11)$$

The high-frequency asymptotic solution of the partial derivative of the Green function takes the form:

$$\left\{ \begin{array}{l} g_{lm}(\mathbf{x}_r, t_0; \mathbf{x}, t) = \frac{1}{\pi} \text{Re} \int_0^\infty d\omega e^{-i\omega(t_0-t)} g_{lm}(\mathbf{x}_r, \mathbf{x}; \omega) \\ \frac{\partial g_{lm}(\mathbf{x}; \mathbf{x}_r; \omega)}{\partial x_k} \approx i\omega \sum_n p_k^n(\mathbf{x}_r) g_{lm}^n(\mathbf{x}; \mathbf{x}_r; \omega) \\ g_{lm}^n(\mathbf{x}; \mathbf{x}_r; \omega) = e_l^n(\mathbf{x}_r) A^n(\mathbf{x}; \mathbf{x}_r) \exp[i\omega T(\mathbf{x}; \mathbf{x}_r)] e_m^n(\mathbf{x}) \end{array} \right. , \quad (12)$$

where $p_k^n(\mathbf{x}_r)$ is the initial slowness of P-wave and SV-wave. $e_l^n(\mathbf{x}_r)$ and $e_m^n(\mathbf{x})$ are the polarity vectors.

Substituting eqs. (10), (11) and (12) into eq. (9), we can obtain the decoupled elastic wave backward continuation formulas of P-wave and SV-wave:

$$u_m^p(\mathbf{x}; \mathbf{x}_r; t_0) = -\int_{t_0}^T dt \frac{\sqrt{\omega_r w_0^2}}{4\pi} \int_{\partial\Omega} \sqrt{\rho(\mathbf{x}_r)} [u_x(\mathbf{x}_r; t) W_1^p(\mathbf{x}_r) + u_z(\mathbf{x}_r; t) W_2^p(\mathbf{x}_r)] dx_r \int e_m^p(\mathbf{x}; \mathbf{x}_r) A^{p*}(\mathbf{x}; \mathbf{x}_r) \exp[-i\omega T^{p*}(\mathbf{x}; \mathbf{x}_r)] \frac{dp_x^p(\mathbf{x}_r)}{p_z^p(\mathbf{x}_r)}, \quad (13)$$

$$u_m^s(\mathbf{x}; \mathbf{x}_r; t_0) = -\int_{t_0}^T dt \frac{\sqrt{\omega_r w_0^2}}{4\pi} \int_{\partial\Omega} \sqrt{\rho(\mathbf{x}_r)} [u_x(\mathbf{x}_r; t) W_1^s(\mathbf{x}_r) + u_z(\mathbf{x}_r; t) W_2^s(\mathbf{x}_r)] dx_r \int e_m^s(\mathbf{x}; \mathbf{x}_r) A^{s*}(\mathbf{x}; \mathbf{x}_r) \exp[-i\omega T^{s*}(\mathbf{x}; \mathbf{x}_r)] \frac{dp_x^s(\mathbf{x}_r)}{p_z^s(\mathbf{x}_r)}, \quad (14)$$

where $W_1^n(\mathbf{x}_r)$ and $W_2^n(\mathbf{x}_r)$ are the weight coefficients, they take the form:

$$\begin{cases} W_1^p(\mathbf{x}_r) = \gamma^2(\mathbf{x}_r) [p_z^p(\mathbf{x}_r) e_x^p(\mathbf{x}_r) + p_x^p(\mathbf{x}_r) e_z^p(\mathbf{x}_r)] \\ W_2^p(\mathbf{x}_r) = p_z^p(\mathbf{x}_r) e_z^p(\mathbf{x}_r) + [1 - 2\gamma^2(\mathbf{x}_r)] p_x^p(\mathbf{x}_r) e_x^p(\mathbf{x}_r) \\ W_1^s(\mathbf{x}_r) = p_z^s(\mathbf{x}_r) e_x^s(\mathbf{x}_r) + p_x^s(\mathbf{x}_r) e_z^s(\mathbf{x}_r) \\ W_2^s(\mathbf{x}_r) = \frac{1}{\gamma^2} p_z^s(\mathbf{x}_r) e_z^s(\mathbf{x}_r) + [1 - 2\gamma^2(\mathbf{x}_r)] p_x^s(\mathbf{x}_r) e_x^s(\mathbf{x}_r) \end{cases}, \quad (15)$$

where γ is the velocity ratio of SV-wave to P-wave.

The forward continuation wavefields characterized by the elastic wave Gaussian beams can be written as:

$$U_m^p(\mathbf{x}; \mathbf{x}_s; t_0) = \frac{i}{4v_p^2(\mathbf{x}_s)} \operatorname{Re} \int_0^\infty d\omega e^{-i\omega t} f(\omega) \sqrt{\frac{\omega_r w_0^2}{\rho(\mathbf{x}_s)}} \times \int \frac{dp_x^p(\mathbf{x}_s)}{p_z^p(\mathbf{x}_s)} A^{p*}(\mathbf{x}; \mathbf{x}_s) \exp[-i\omega T^{p*}(\mathbf{x}; \mathbf{x}_s)] \quad (16)$$

The anisotropic imaging formula of converted PS-wave

Fig. 2 shows the propagation process of converted PS-wave. The displacement components of converted PS-wave at the reflection points O_1 and O_2 are opposite because of the different incident angles. Therefore, the X -components of seismic records received at R_1 and R_2 have opposite polarities. In the proposed method, we introduce a symbol function according to the incident angle to implement the polarization correction in the imaging results directly.

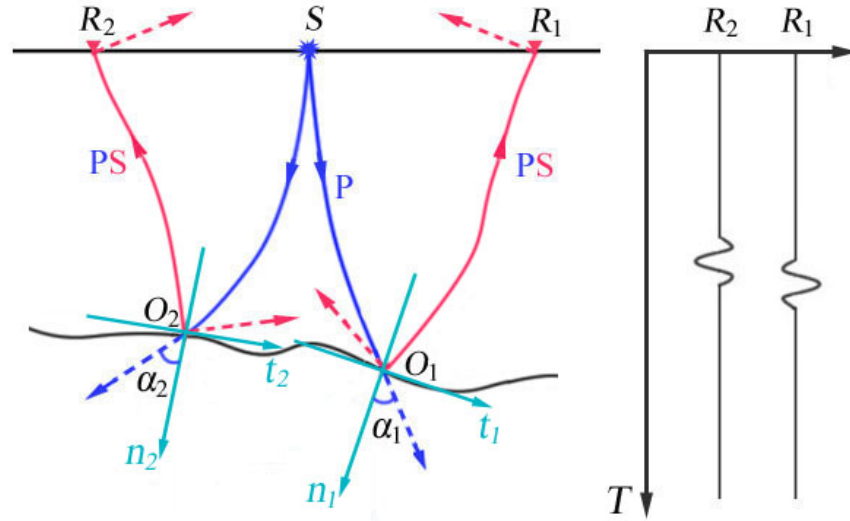


Fig. 2. The polarization of converted PS-wave at the reflector.

According to the reflection imaging principle (Claerbout, 1971), the imaging formula of converted PS-wave takes the form:

$$I^{ps}(\mathbf{x}; \mathbf{x}_s) = -\frac{i\omega_r w_0^2}{16\pi v_p^2(x_s)} \int dt_0 \int_{\partial\Omega} \sqrt{\frac{\rho(\mathbf{x}_r)}{\rho(\mathbf{x}_s)}} dx_r \iint \frac{dp_x^p(\mathbf{x}_s) dp_x^s(\mathbf{x}_r)}{p_z^p(\mathbf{x}_s) p_z^s(\mathbf{x}_r)} \text{sgn}(\alpha) \quad (17)$$

$$\times u_{GBz}^p(\mathbf{x}; \mathbf{x}_s) u_{GBx}^s(\mathbf{x}; \mathbf{x}_r) [u_x(\mathbf{x}_r; t) W_1^s(\mathbf{x}_r) + u_z(\mathbf{x}_r; t) W_2^s(\mathbf{x}_r)]$$

NUMERICAL EXAMPLES

Fault model

In this section, we use the Fault model to test the effectiveness of the proposed method. The model consists of a fault and two horizontal layers with different anisotropic parameters, as shown in Fig. 3. The vertical and horizontal grid points are 301 and 1801 with a 10 m spacing. The synthetic seismogram is generated using anisotropic ray tracing forward modelling method, and the source wavelet is the Ricker wavelet with a dominant frequency of 25 Hz. There are 281 shot records received on the surface with 50 m interval. There are 201 receivers per shot with a 20 m tracing interval. The recording time is 3.0 s with a 1ms sampling interval. Fig. 4 shows the X-component and Z-component of the shot record.

The imaging result obtained by the isotropic converted PS-wave reverse time migration with Gaussian beams is shown in Fig. 5a, where the fault is

not accurately imaged. There are defocusing artifacts and imaging noise around the reflection interfaces. The events apparently curve up at the edge of the anisotropic layers. Figs. 5b and 5c display the imaging results using anisotropic reverse time migration with Gaussian beams based on elastic parameters and the proposed method, respectively. Both of the imaging results are excellently matched with the exact model. The anisotropic layers are clearly depicted and the imaging noise is eliminated. However, due to the different ray tracing equations, the events in the imaging result obtained by the proposed method are better focused and continuous, especially around the fault. The comparison of computational efficiency is shown in Table 1. From the calculation time of single shot, we can know the proposed method has a higher computational efficiency than that of the method based on elastic parameters. The comparison of the imaging results and computational efficiency indicate the effectiveness of the proposed method.

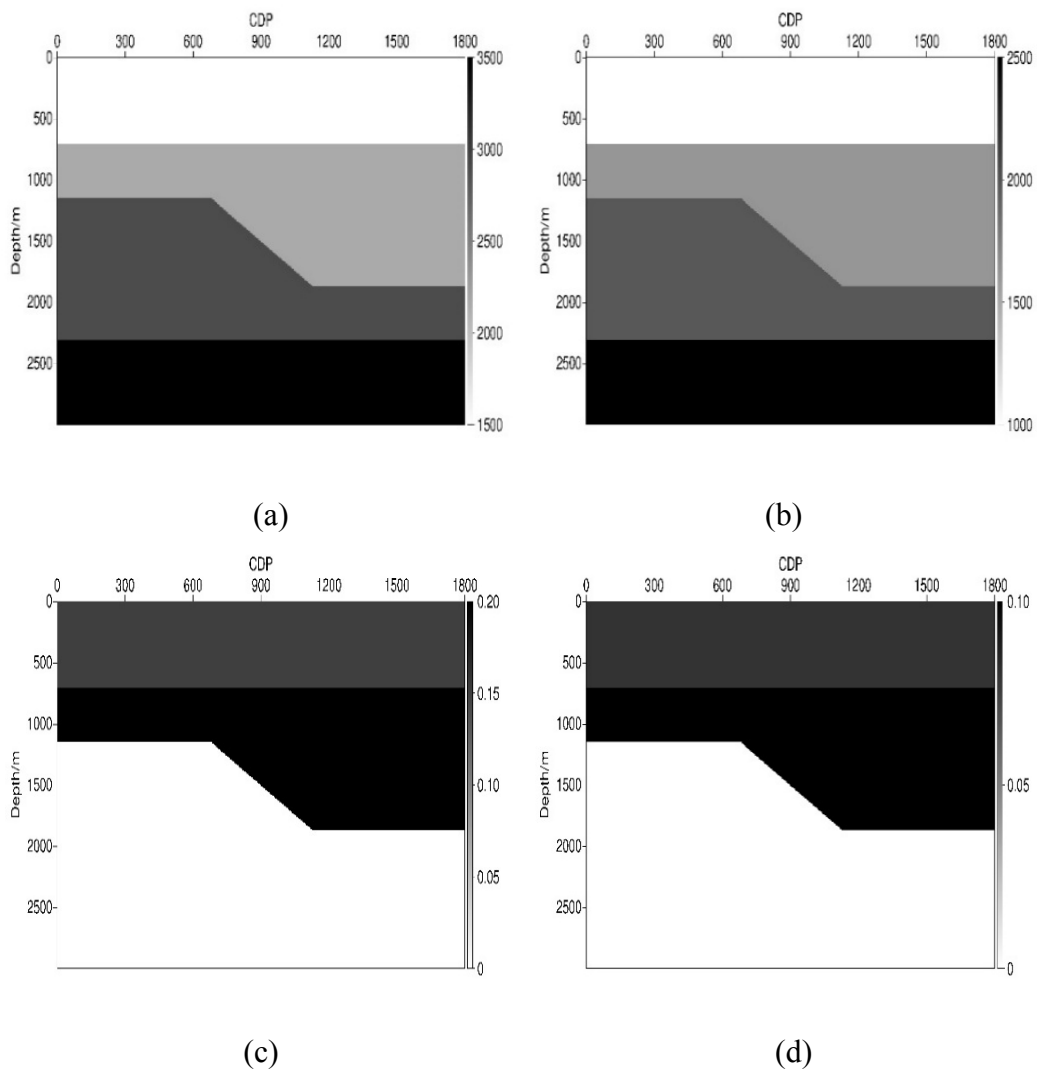


Fig. 3. Fault model. (a) The velocity field of P-wave. (b) The velocity of SV-wave. (c) Epsilon. (d) Delta.

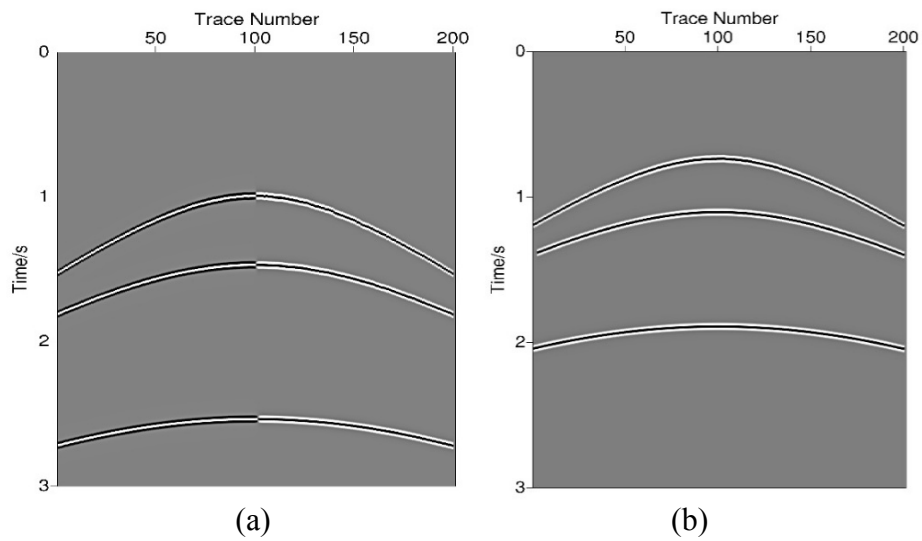


Fig. 4. The shot record at CDP 251: (a) X-component; (b) Z-component.

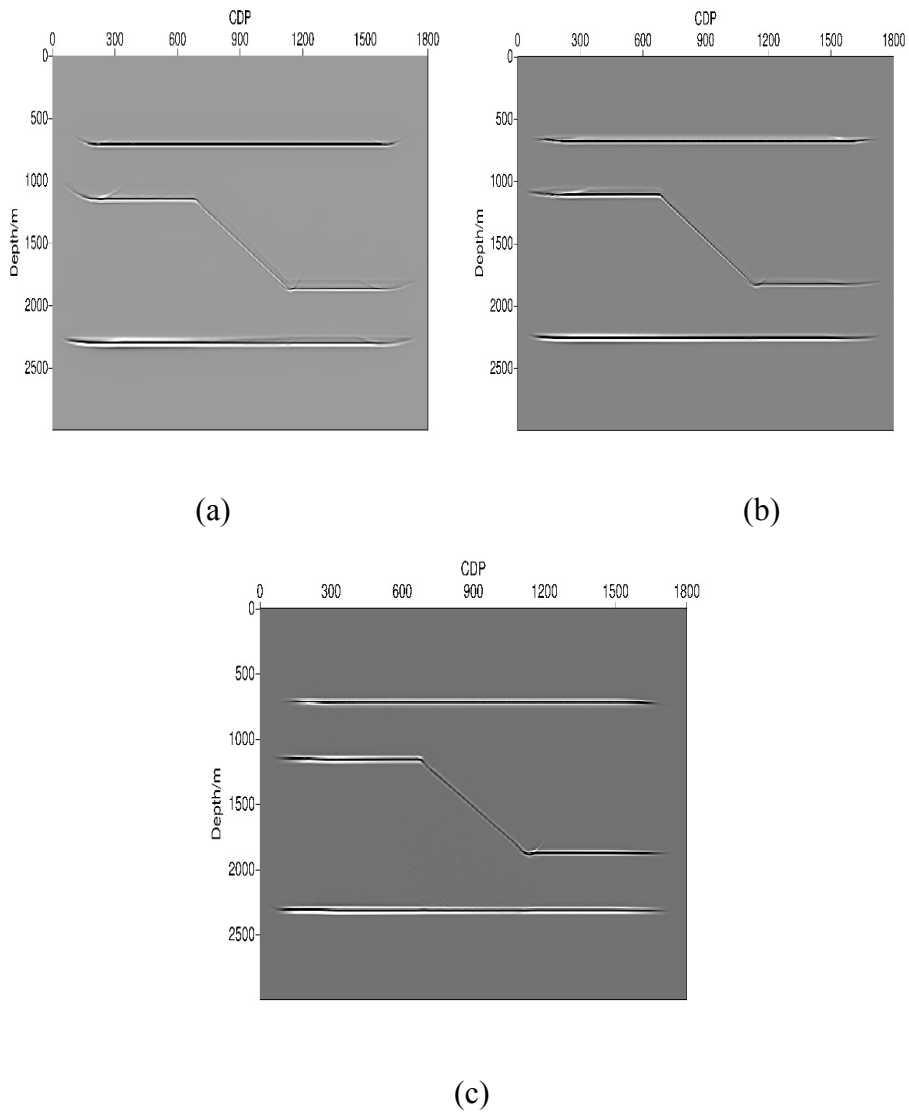


Fig. 5. Imaging results of the fault model: (a) The isotropic method; (b) The anisotropic method (based on elastic parameters); (c) The proposed method.

Table 1. The comparison of computational efficiency.

Methods	The calculation time of per shot
The isotropic method	118.2 s
The anisotropic method based on elastic parameters	142.8 s
The proposed method	125.6 s

SL model

Next, the applicability of the proposed method is demonstrated on a SL model. There are five layers (including inclined layers, relief structures, etc.) in the model with different anisotropic parameters, as shown in Fig. 6. The model is 3.5 km deep and 14.01 km long, with 10 m grid spacing. The anisotropic ray tracing forward modelling method is used to generate the synthetic seismogram. The source wavelet is Ricker wavelet with a dominant frequency of 25 Hz. The synthetic seismogram consists of 251 shot records with 301 receivers per shot. There are 4001 time sampling points, the sampling interval is 1 ms. The shot record is displayed in Fig. 7.

We also use three methods (the isotropic method, the method based on elastic parameters, the proposed method) to test the model. The imaging result obtained by isotropic method is shown in Fig. 8a. Due to the neglect of anisotropic factors, the inclined layers and relief structures are not imaged at the true position. The defocusing effects around reflectors are also visible in the imaging result and the events of the reflectors are not well focused (as indicated by the box). Figs. 8b and 8c display the imaging results using the anisotropic method based on elastic parameters and the proposed method, respectively. Clearly, the migration results in Figs. 8b and 8c are better than that of Fig. 8a. The structures are well positioned and the defocusing effects around the reflectors are also eliminated. Compared Figs. 8b with 8c, it can be seen that the proposed method has a better imaging quality, where the energy of events are more uniform distribution.

To further display the influence of anisotropy on converted PS-wave imaging, we extract the ADCIGs located at CDP = 701. The events in the ADCIGs extracted by isotropic method (as shown in Fig. 9a) are not located at the true position and obviously curve up at large incidence angles. While in the ADCIGs extracted by anisotropic methods, the events are flat and well positioned, as shown in Figs. 9b and 9c. And the events in the proposed method are more focused and continuous than that of the method based on elastic parameters.

From the comparison of the imaging results and ADCIGs, we can conclude that the proposed method can provide a better imaging quality than that of the isotropic method and the anisotropic method based on elastic parameters.

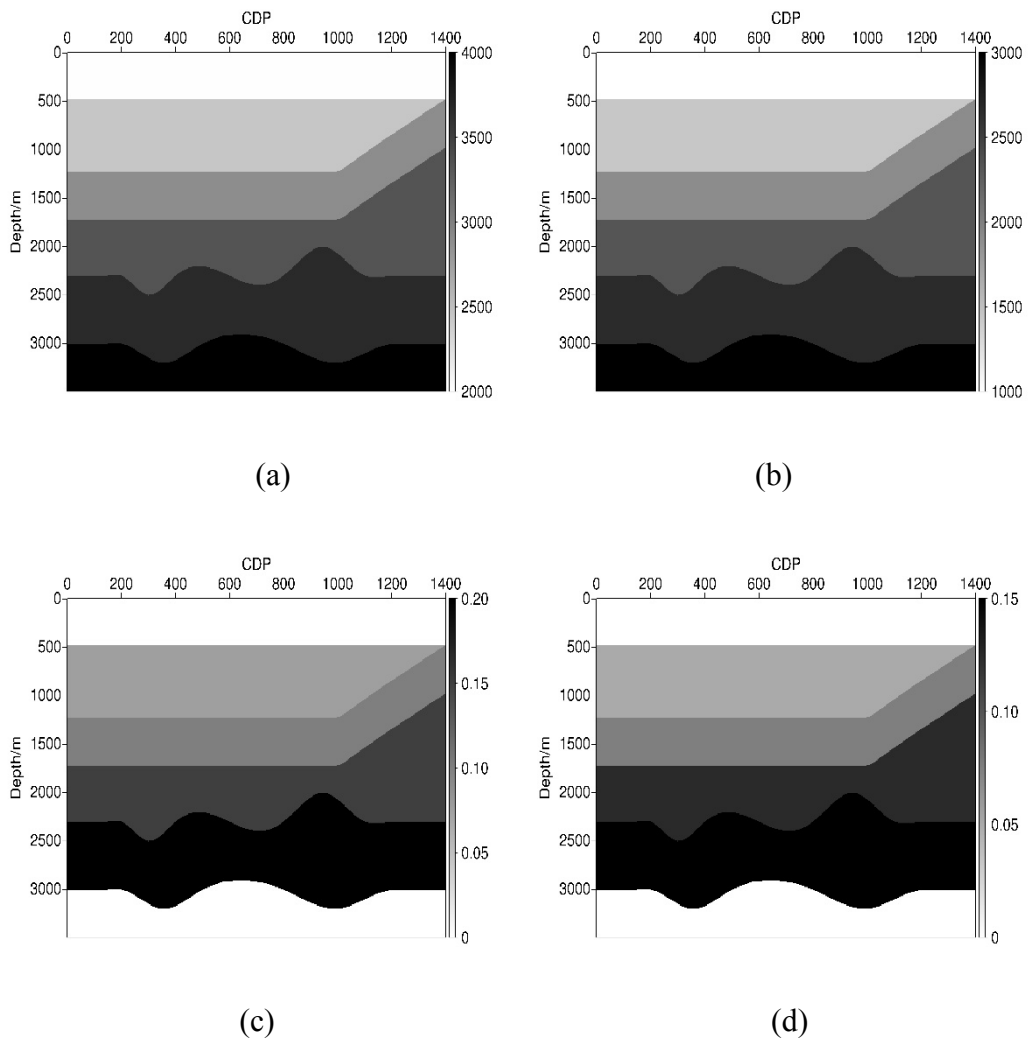


Fig. 6. SL model: (a) The velocity field of P-wave; (b) The velocity of SV-wave; (c) Epsilon; (d) Delta.

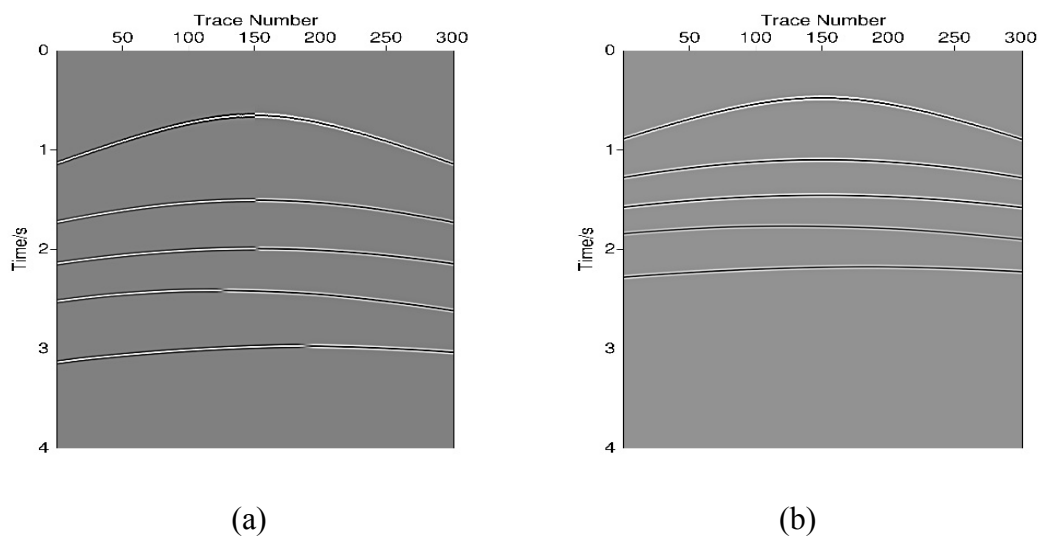


Fig. 7. The shot record at CDP 541: (a) X-component; (b) Z-component.

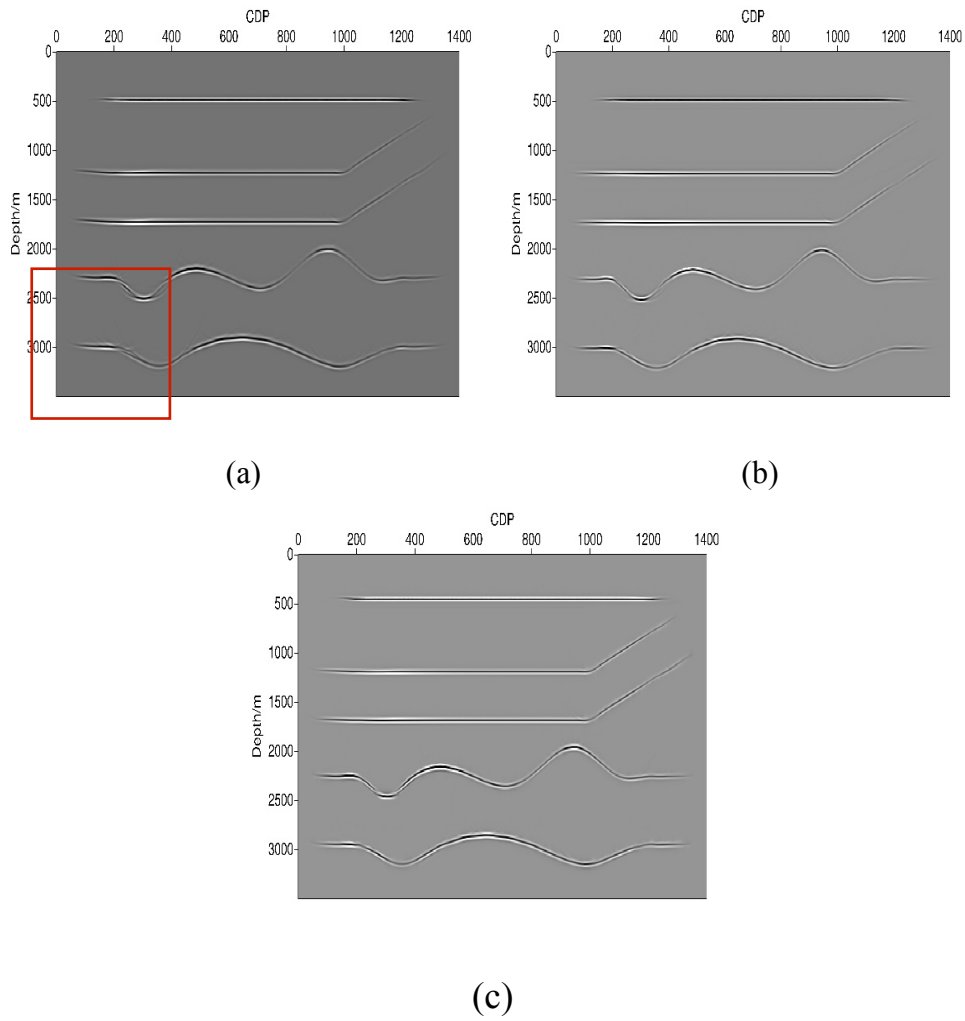


Fig. 8. Migration results of SL model: (a) The isotropic method; (b) The anisotropic method (based on elastic parameters); (c) The proposed method.

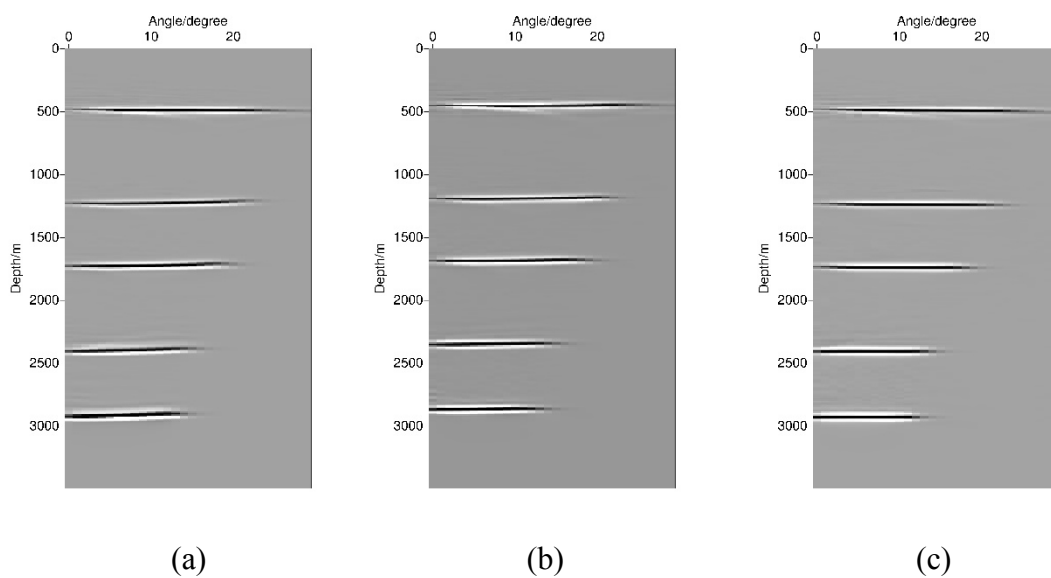


Fig. 9. The extracted ADCIGs of SL model at CDP=701: (a) The isotropic method; (b) The anisotropic method (based on elastic parameters); (c) The proposed method.

CONCLUSIONS

By modifying the anisotropic kinematic and dynamic ray tracing equations, we develop an anisotropic converted PS-wave ray tracing algorithm and apply it to the converted wave imaging. We adopt the elastic wave Gaussian beams to construct the Green function, then realize the forward continuation and backward continuation of wavefields, and finally the imaging results are obtained through the reflection imaging principle. According to converted PS-wave propagation characteristics, we also introduce a symbolic function to implement the polarization correction in imaging results directly. Through the numerical tests we can know that the proposed method not only has a higher computational efficiency, but also can image the anisotropic structures accurately.

ACKNOWLEDGEMENTS

This research is supported by the National Natural Science Foundation of China (no. 41504100, 41374122). Thanks for the support and help from the Seismic Wave Propagation and Imaging (SWPI) research group of China University of Petroleum (East China)! Thanks to the editorial department teachers and reviewers for this article given guidance and suggestions!

REFERENCES

- Alfaraj, M. and Lerner, K., 1992. Transformation to zero offset for mode-converted waves. *Geophysics*, 57: 474-477.
- Alkhalifah, T., 1995. Gaussian beam depth migration for anisotropic media. *Geophysics*, 69: 1474-1484.
- Babič, V.M. and Kirpičnikova, N.Y., 1980. The Boundary-Layer method in diffraction problems. *Optica Acta Internat. J. Optics*, 27: 282-282.
- Baysal, E., Dan, D.K. and Sherwood, J.W.C., 1983. Reverse time migration. *Geophysics*, 48: 1514-1524.
- Bi, L.F., Qin, N. and Yang, X.D., 2015. Gauss beam reverse time migration method for elastic multiple wave. *Geophys. Prosp. Petrol.* (in Chinese), 54: 64-70.
- Červený, V., 1972. Seismic rays and ray intensities in inhomogeneous anisotropic media. *Geophys. J. Internat.*, 29: 1-13.
- Červený, V., Popov, M.M. and Pšenčík, I., 1982. Computation of wave fields in inhomogeneous media - Gaussian beam approach. *Geophys. J. Internat.*, 70: 109-128.
- Dai, H. and Li, X.Y., 2006. The effects of migration velocity errors on traveltimes accuracy in prestack Kirchhoff time migration and the image of PS converted waves. *Geophysics*, 71(2): S73-S83.
- Guitton, A., Kaelin, B. and Biondi, B., 2006. Least - square attenuation of reverse time migration artifacts. *Geophysics*, 72(1): S19.
- Gray, S.H., 2005. Gaussian beam migration of common-shot records. *Geophysics*, 70(4): S71-S77.
- Gray, S.H. and Bleistein, N., 2009. True-amplitude Gaussian-beam migration. *Geophysics*, 74(2): S11-S23.
- Han, J., Wang, Y., Xing, Z. and Lu, J., 2014. Gaussian beam prestack depth migration of converted wave in TI media. *J. Appl. Geophys.*, 109: 7-14.

- Hanyga, A., 1986. Gaussian beams in anisotropic elastic media. *Geophys. J. Internat.*, 85: 473-504.
- Hill, N.R., 1990. Gaussian beam migration. *Geophysics*, 55: 1416-1428.
- Hill, N.R., 2001. Prestack Gaussian-beam depth migration. *Geophysics*, 66: 1240-1250.
- Huang, J.P., Zhang, Q., Zhang, K., Li, Z.C., Yue, Y.B. and Yuan, M.L., 2014. Reverse time migration with Gaussian beams based on the Green function. *Oil Geophys. Prosp.*, 49: 101-106.
- Li, X., Dai, H. and Mancini, F., 2007. Converted-wave imaging in anisotropic media: theory and case studies. *Geophys. Prosp.*, 55: 345-363.
- Nowack, R.L., Sen, M.K. and Stoffa, P.L., 2003. Gaussian beam migration for sparse common-shot and common-receiver data. *Expanded Abstr.*, 73rd Ann. Internat. SEG Mtg., Dallas.
- Pao, Y.H. and Varatharajulu, V., 1976. Huygens' principle, radiation conditions, and integral formulas for the scattering of elastic waves. *J. Acoust. Soc. Am.*, 59: 1361-1371.
- Popov, M.M., Semtchenok, N.M., Popov, P.M. and Verdel, A.R., 2010. Depth migration by the Gaussian beam summation method. *Geophysics*, 75(2): S81.
- Rooijen, H.P.G.M., 1991. Stacking of P-SV seismic reflection data using DIP moveout. *Geophys. Prosp.*, 39: 585-598.
- Sun, W., Zhou, B. and Fu, L.Y., 2010. Dip angle-compensated one-way wave equation migration. *Explor. Geophys.*, 41: 137-145.
- Tessmer, G., Krajewski, P., Fertig, J. and Behle, 1990. Processing of PS-reflection data processing of PS-reflection data applying a common conversion-point stacking technique. *Geophys. Prosp.*, 38: 267-268.
- Thomsen, L., 1986. Weak elastic anisotropy. *Geophysics*, 51: 1954-1966.
- Wang, W., Pham, L.D. and Lou, M., 2002. Converted-wave prestack time migration for isotropic and anisotropic media. *Expanded Abstr.*, 72nd Ann. Internat. SEG Mtg., Salt Lake City.
- Yu, Z., Xu, S., Zhang, G. and Bleistein, N., 2007. True amplitude turning-wave one-way wave equation migration. *Geophys. Prosp. Petrol.*, 46: 582-581.
- Yue, Y.B., 2011. Study on Gaussian beam migration methods in a complex medium. Qingdao: China University of Petroleum (East China).
- Zai-Tian, M.A., 1995. Two-dimensional elastic wave migration of common offset seismic section. *Chin. J. Geophys.*: S1.
- Zhang, K., Duan, X.Y., Li, Z.C., Huang, J.P. and Zhang, Q., 2015. Angel domain reverse time migration with Gaussian beams in anisotropic media. *Oil Geophys. Prosp.*, 50: 912-918.
- Zhu, T., Gray, S.H. and Wang, D., 2005. Kinematic and dynamic raytracing in anisotropic media: theory and application. *Expanded Abstr.*, 75th Ann. Internat. SEG Mtg., Houston.
- Zhu, T., Gray, S.H. and Wang, D., 2007. Prestack Gaussian-beam depth migration in anisotropic media. *Geophysics*, 72(3): S133-S138.